NJC

PAPER

View Article Online
View Journal

Check for updates

Cite this: DOI: 10.1039/c9nj00347a

Energy framework approach to the supramolecular reactions: interplay of the secondary bonding interaction in Ph_2E_2 (E = Se, Te)/*p*-I-C_6F_4-I co-crystals†

Yury V. Torubaev,*[a] Dhirendra K. Rai,[b] Ivan V. Skabitsky,[a] Srimanta Pakhira[bc] and Artem Dmitrienko[d]

Received 20th January 2019,
Accepted 15th April 2019

DOI: 10.1039/c9nj00347a

rsc.li/njc

In the co-crystals of diphenyl dichalcogenides Ph_2E_2 (E = Se, Te), the E–E and E–π(Ph) chalcogen bonds assemble Ph_2E_2 molecules into the chains, which imitate the typical packing patterns of the parent Ph_2E_2 crystals. These co-crystals consist of quite stable tectonic 1D and 2D Ph_2E_2 chain architectures, which are repeated in the crystals of pure Ph_2E_2 as well as in their co-crystals with the halogen bond donor molecules. These chains can be clearly visualized as separate parallel 1D and 2D structures in the energy framework diagrams in CrystalExplorer. From this point of view, the supramolecular reaction of Ph_2E_2 with the halogen bond donor 1,4-diiodotetrafluorobenzene (*p*-DITFB) can be considered as the insertion of *p*-DITFB molecules between the Ph_2E_2 chains in such a way that I–E and I–π(Ph) halogen bonds come in place of E–E and Te–π(Ph) chalcogen bonds, which are responsible for the close packing of these chains in the parent crystal form. Persistent packing patterns found in parent and binary crystals can provide insight into the mechanism of the crystallization process.

Introduction

Uncovering the fundamentals of the molecular crystal formation and composition remains one of the most common challenges of chemistry in the new century, and becomes even more important with the shift in its focus to the noncovalent interactions.[1] Molecular co-crystals of two or more components, assembled by relatively strong, directed, tunable and specific attractive interactions, offer a wide field for the theoretical and experimental modeling. Such studies have led to a significant advancement in the understanding of the mechanisms governing self-assembly of the molecules into stable structures with tunable properties.[2,3] A relatively new class of secondary bonding interactions (SBI), which corresponds to the above requirements for energy, directionality, tunability, and specificity, is halogen bonding (XB).[4] The well-established close analogues of halogen bonds are chalcogen bonds (ChB),[5] pnictogen bonds (PB)[6] and other σ-hole interactions. The combinations of the molecules bearing both XB and ChB donor/acceptor sites are expected to offer an interesting subject to study the underlying fundamentals of self and intermolecular assemblies.

While identifying the supramolecular assemblies and the structural patterns in the solid state, we should keep in mind the subjective nature of any discrete assemblies or structural motifs one can see in a solid-state framework.[7,8] However, the idea of proposing a structural pattern just based on seemingly obvious supramolecular aggregates and not supported by appropriate intermolecular energy calculations can be misguiding. For example, the packing pattern of some substituted benzenes may quite obviously and convincingly look like a layered structure, but the computations of the topology of intermolecular interactions indicate that these crystals are, in fact, columnar with weak interactions between the columns.[9] This approach also allowed for the rationalization of the physical properties of the crystals, but the high computation cost restricted its use. Later, a similar approach to understand the crystal packing, based on intermolecular interaction energies but combining the more efficient calculation instrument with the graphical representation of

[a] N. S. Kurnakov Institute of General and Inorganic Chemistry, Russian Academy of Sciences, GSP-1, L eninsky prospect, 31, 119991 Moscow, Russia. E-mail: torubaev@igic.ras.ru; Tel: +7 495 954 38 41
[b] Discipline of Metallurgy Engineering and Materials Science, Indian Institute of Technology, Simrol, Indore, India
[c] Department of Chemical & Biomedical Engineering, Florida A&M – Florida State University, Joint College of Engineering, 2525 Pottsdamer Street, Tallahassee, Florida, 32310, USA
[d] A. N. Nesmeyanov Institute of Organoelement Compounds, Russian Academy of Sciences, Moscow, Russia

† Electronic supplementary information (ESI) available. CCDC 1815996 (**1**), 1815995 (**2**). For ESI and crystallographic data in CIF or other electronic format see DOI: 10.1039/c9nj00347a

their magnitude, was introduced as 'energy frameworks',[10] and featured in the Crystal Explorer software.[11] The energy frameworks were effectively used to investigate the nature of chalcogen bonding in Ph_2E_2 (E = Se, Te),[12] structure,[13] topology of supramolecular recognition,[14,15] and physical properties[16–21] of the crystals. The present study extends the application of the crystal energy framework analysis for the study of supramolecular reactions, particularly, the interaction of diphenyldichalcogenides Ph_2E_2 (E = Se, Te) with XB-donor 1,4-diiodotetrafluorobenzene (*p*-DITFB).

Results and discussion

The co-crystallization of Ph_2Te_2 with 1,4-diiodotetrafluorobenzene (*p*-DITFB) resulted in elongated prismatic $P2_1/n$ orange crystals comprising 1 : 1 combination of both co-formers (**1**, see Fig. 1a). In **1**, Ph_2Te_2 molecules assembled into the chains similar to those in parent Ph_2Te_2 crystals (see Fig. 1a–c and Fig. S5, ESI†).

General consideration of p-orbital symmetry in chalcogens, supported by calculations for highly polarized systems like SCl_2,[23]

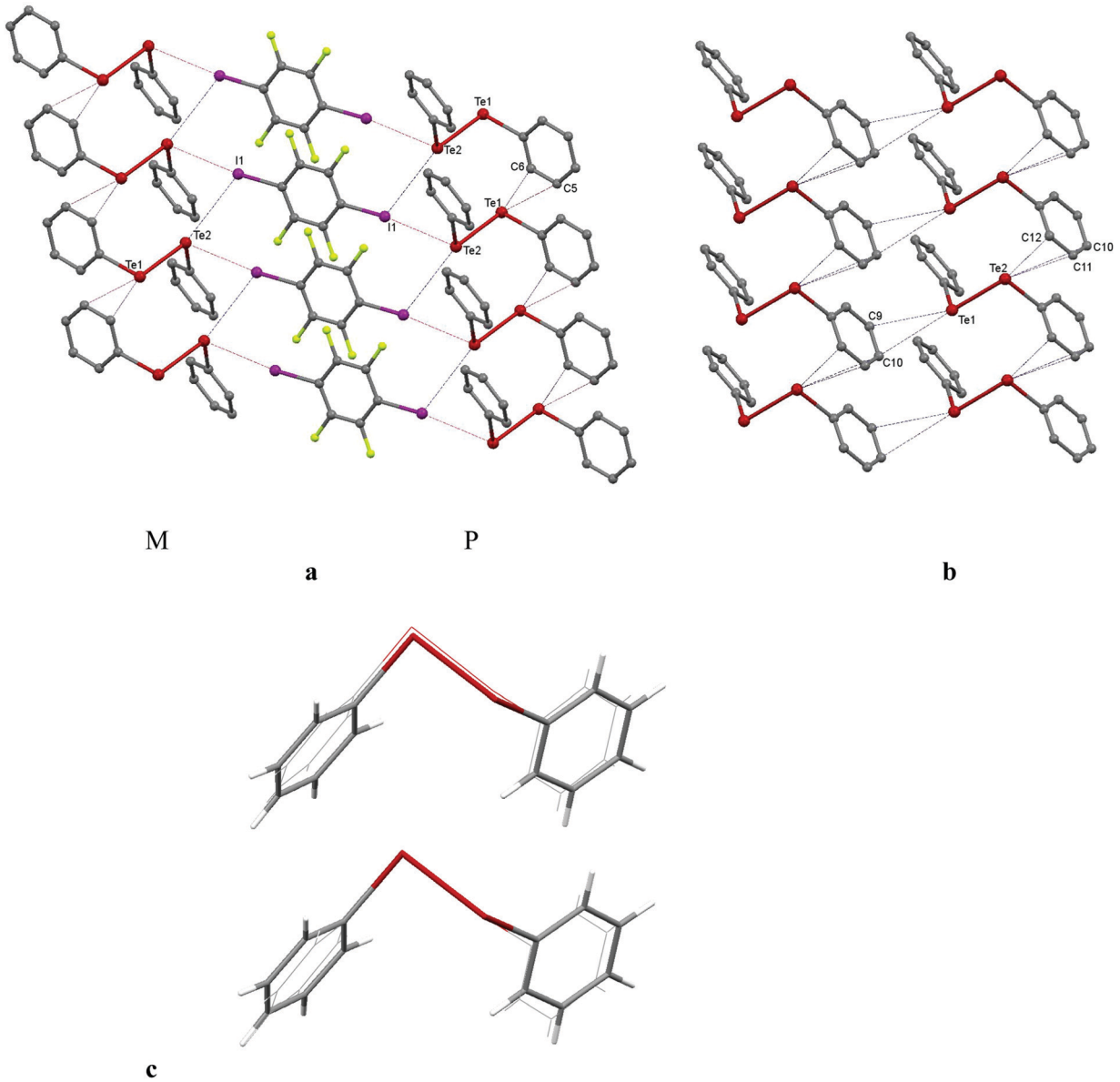

Fig. 1 (a) Fragment of the packing diagram of **1** showing the presence of both Te–πPh ChBs and I–Te XBs and two enantiomeric P and M molecules, arranged into separate homochiral chains, which are linked by *p*-DITFB. Selected intermolecular distances (Å): I1–Te2 3.5736(3), Te1–Te2 4.3125(3), I1–Te2 4.0308(3), Te1–C5 3.454(3), and angles (°): C13–I1–Te2 174.13(7), Te1–Te2–I1 99.83(1), Te1–Te2 I1 165.94(1). (b) Fragment of the packing diagram of native Ph_2Te_2 (DPHDTE01) showing Ph_2Te_2 molecules assembled into the chains, through the Te–π(Ph) and Te–Te ChBs, which are linked by Te–C ChBs. Selected intermolecular distances (Å): Te(2)–C(11) 3.591(6), Te(1)–Te(2) 4.181(1), Te(1)–C(9) 3.740(6), Te(1)–C(10) 3.643(5), Te(1)–Te(1) 5.152(2) and angles (°): Te(2)–Te(1)–Te(2) 94.51, Te(2)–Te(1)–C(2) 171.96, Te(1)–Te(2)–C(2) 170.26. (c) Structure overlay (in CCDC Mercury[22]) of the Ph_2Te_2 chain fragments in the parent Ph_2Te_2 crystal (YUXQEO) and co-crystal **1** (wireframe).

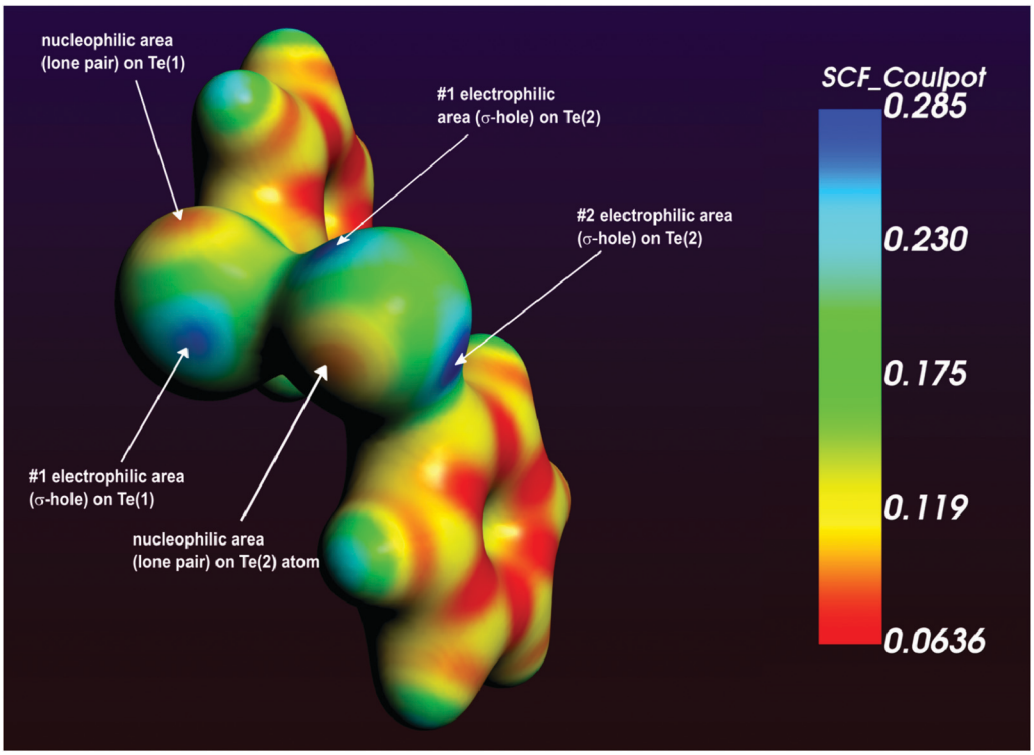

Fig. 2 (a) ESP map of the isolated Ph_2Te_2 molecule, reproducing its conformation in the co-crystal **1**, showing two different σ-holes on each Te atom, *trans* to Te–Te bond and *trans* to the Te–C bond. Note the orthogonal orientation of the Ph planes towards the Te–Te bond and well pronounced nucleophilic (orange-yellow) areas on Te atom, corresponding to its lone pair.

SeF_2,[24] $(CF_3)_2Se$,[25] indicate that the E^{II} chalcogen atom can have two σ-holes. In the less electronegative and asymmetric environment, the σ-holes may appear less pronounced (may differ from one another) but are still quite apparent.[26] Two positive areas on each of the chalcogen atoms in Ph_2E_2 (E = S, Se, Te) steadily increase down the group (S < Se < Te) (see Fig. S2, ESI†). Fig. 2 depicts the ESP map of Ph_2Te_2, where two unequal σ-holes on each Te atom can be clearly seen. The most positive one, which is positioned *trans* to the Te–Te bond, forms short and relatively strong Te–π(Ph) chalcogen bonds in parent Ph_2Te_2 (Te–C 3.591(6) – 3.643(5) Å/−1.05 kcal mol^{-1}) and **1** (Te–C 3.454(3) – 3.627(3)Å/ −1.30 kcal mol^{-1}) neighbors. The second one, positioned *trans* to the Te–C bond, is significantly less pronounced and, therefore, quite naturally forms elongated and weaker Te–Te ChB (4.181(1) Å/ −0.24 kcal mol^{-1}) in parent Ph_2Te_2 and **1** (Te1–Te2 4.3125(3) Å).

The adjacent Ph_2Te_2 stacks are connected by the *p*-DITFB linker and, quite naturally, the nucleophilic area of the iodine atom of *p*-DITFB is approaching the σ-hole of the Te2 atom located *trans* to the Te–Te bond. These σ holes are less shielded and, therefore, are less involved in other XBs/ChBs,[27] leaving the Ph_2Te_2 chain architecture intact. Additional stabilization of *p*-DITFB-Ph_2Te_2 assembly is achieved by the bonding of the same iodine function to the nucleophilic area of Te2 atom (4.0308(3) Å) (see Fig. 1a) of the adjacent Ph_2Te_2 molecule in the same stack, so that *p*-DITFB appears in its less common *emploi* of Te–I XB acceptor.‡

‡ (Te–Te–I and Te–I–C) angles (99.83(1)° and 174.13(7)°), respectively, are corresponding the type II contact, *i.e.* genuine XB.

These halogen I–Te (−2.27 kcal mol^{-1}) and chalcogen Te–I (−0.74 kcal mol^{-1}) bonds in Ph_2Te_2– *p*-DITFB assembly, formally come in place of pairs of Te–π(C–C) (−0.82 kcal mol^{-1}) ChB and Te–H (−0.69 kcal mol^{-1}) between the chains in parent Ph_2Te_2 (3.04 kcal mol^{-1}) (see Fig. 1a and Tables S1 and S2, ESI†). Taking into account the additional C–H, I–H, F–C and H–H interactions, the inter-chain interaction in co-crystal **1** (−4.16 kcal mol^{-1}) is further significantly stabilized as compared to parent Ph_2Te_2 (−3.04 kcal mol^{-1}).

In terms of the Atoms in Molecules (AIM) formalism, the weak intermolecular bonding interactions take place at the bond critical point (3,−1) and their energies (E_{cont}) can be predicted with high accuracy using the basis of the potential energy density function $v(r)$ – the correlation suggested by Espinosa *et al.* (CEML).[28] Recently, the physical interpretation of CEML was suggested[29] and such correlation was found to be valid for coordinate bonds Gd–X (X = O, N, Cl),[30] Au–P,[31] Pd–C,[32] and Ru–(C_5H_5).[33] The QTAIM analysis in conjunction with Espinosa's correlation scheme (CEML) for the intermolecular interactions in parent Ph_2E_2 (E = Se, Te) and their co-crystals **1** and **2** demonstrated that the partial energy of chalcogen–chalcogen or chalcogen-element interactions is not always the strongest when compared with that of H–C, H–Ch and other hydrogen bonding interactions (ESI†). In the native Ph_2Te_2 crystal and its *p*-DITFB derivative **1**, the Te–Ph (−1.05 and −1.30 kcal mol^{-1}, respectively) and the Te–Te (−0.62 and 0.48 kcal mol^{-1}, respectively) interactions account almost for half of the interaction energy between the pair of molecules in the stack (−3.46 and

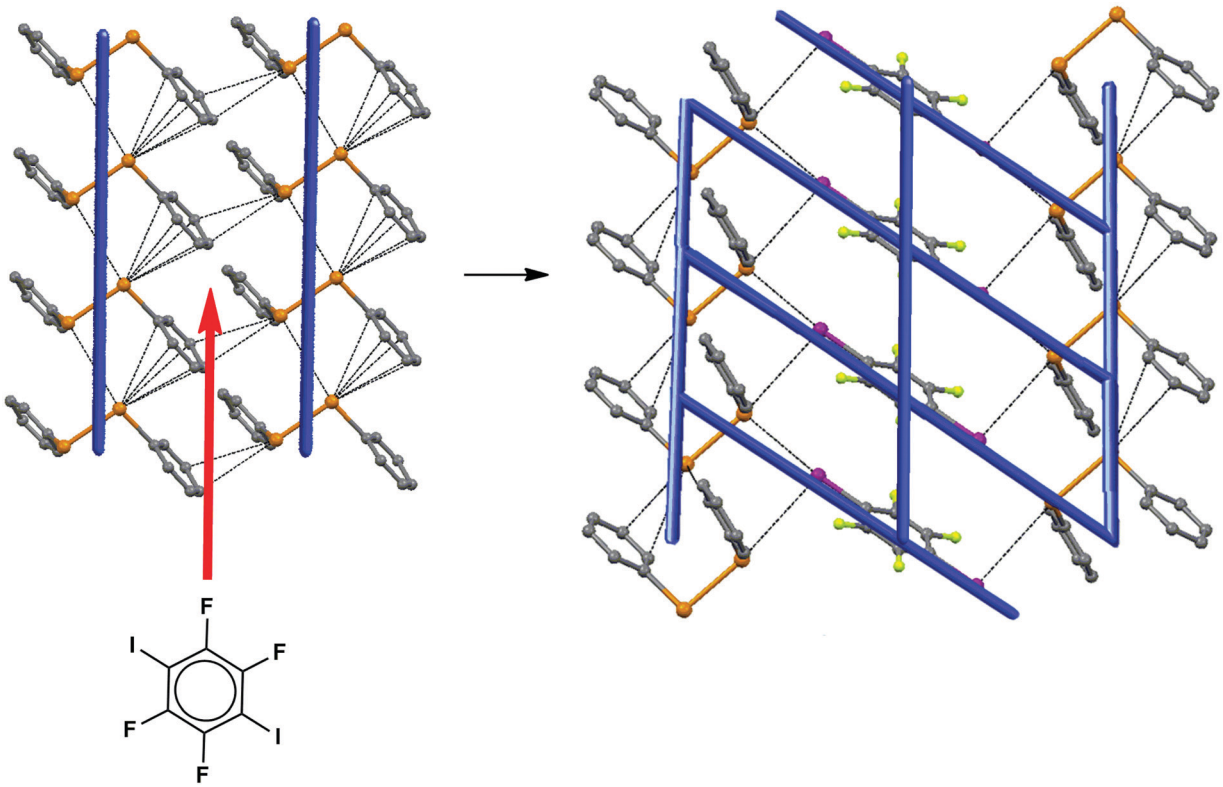

Fig. 3 Supramolecular insertion of *p*-DITFB into the voids in the energy framework (not the crystal lattice) of Ph_2Te_2 resulting in co-crystal **1**. Solid blue cylinders show total energy§ framework (Crystal Explorer 17.5, cut-off 10 kJ mol^{-1}). Black dotted lines show intermolecular bonding.

−3.84 kcal mol^{-1}). However, this is not a general case for the other supramolecular aggregates, which can be identified in these crystals. The contributions of the interactions between these chains with the intermolecular Ph_2Te_2–Ph_2Te_2 bonding in the native crystal (−2.23 kcal mol^{-1}) is only 10% from the Te–Te bonding (−0.24 kcal mol^{-1}), while the remaining 90% is due to the hydrogen bonding interactions. However, the molecular architectures built up with the significant contribution of chalcogen–element interactions are those which reappear in their co-crystals. Although QTAIM\CEML and Crystal Explorer 17.5 (TONTO B3LYP-DGDZVP) energy data do not fully match, they are in good agreement while determining the stronger intermolecular interactions (see Table S4, ESI†). The energy framework approach of Crystal Explorer[34] allowed to visualize a similarity in the framework of the strongest intermolecular interactions in Ph_2Te_2 and its co-crystal **1** (see Fig. 3).

The corresponding supramolecular insertion of *p*-DITFB chains between the chains of Ph_2Te_2 molecules can be presented using this approach so that *p*-DITFB molecules fit into the "voids" in the energy framework (not the crystal lattice) of the parent Ph_2Te_2 crystal (see Fig. 3).

As a final remark on **1** packing pattern, it should be noted that two energetically indistinguishable enantiomeric forms of Ph_2Te_2 yield the two separate chiral crystal forms P and M[35] (see Scheme 1).

In the racemic co-crystal **1** ($P2_1/c$), both P and M enantiomers are assembled into parallel stacks of homochiral Ph_2Te_2 molecules, which are linked by *p*-DITFB molecules (see Fig. 1). The low torsion barrier for Ph–Te–Te–Ph demonstrated in 29 suggests an easy achievement of 50 : 50 distribution of M and P enantiomers in the solution and the stabilization of homochiral stacks by Te–π(Ph) interactions upon the co-crystallization with *p*-DITFB.

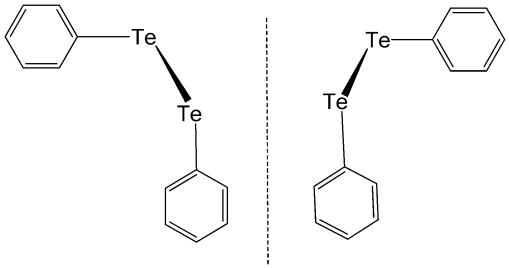

Scheme 1 P and M enantiomeric forms of Ph_2Te_2 (YUXQEO and DPHDTE01, respectively).

In the same way as Ph_2Te_2 1D-chains in **1** replicate the chain pattern in the parent Ph_2Te_2, the Se–Se chalcogen bonded zig-zag chains of Ph_2Se_2 in its pure crystalline form 29 were found in the co-crystals of Ph_2Se_2 with DITFB (**2**), (see Fig. 4 and Fig. S6, ESI†).

2D Ph_2Se_2 chains in the parent crystal, additionally stabilized by the dense network of intermolecular Se–Se ChBs (−2.0 and −3.5 kcal mol^{-1}), are associated with one another by H–Se (−2.6 kcal mol^{-1}) and H–(Ph) (−2.4 kcal mol^{-1}) from one side and H–(Ph) (−4.1 kcal mol^{-1}) HBs from the other. The latter

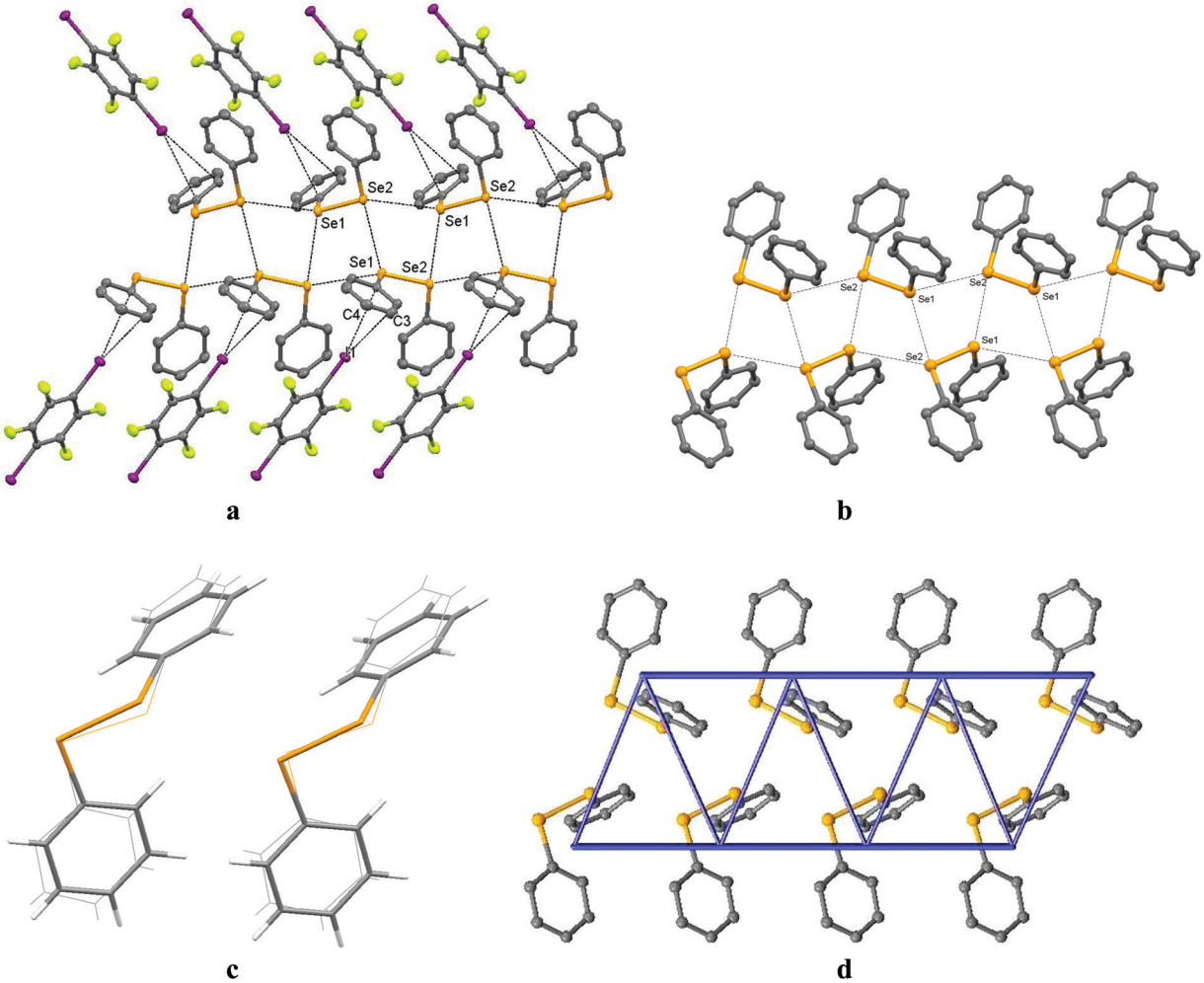

Fig. 4 (a) Fragment of the packing diagram of **2** showing the presence of both Se–Se ChBs and H–πPh HBs. Selected intermolecular distances (Å): Se1–Se2 3.7524(5); Se1–Se2 3.6056(4); I1–C3 3.729(3); C2–I1 3.548(3). (b) Fragment of the packing diagram of parent Ph_2Se_2 (YUXPIR[29]) showing its molecules assembled into the 2D zig-zag chain through the Se–Se ChBs. Selected intermolecular distances (Å): Se2 (*x*, *y*, *z*)–Se1 (−1 + *x*, *y*, *z*) 3.764, Se1(*x*, *y*, *z*)–Se1(*x* − 1/2 + *x*, 1.5 − *y*, 1−*z*) 3.788 (c) structural overlay of the Ph_2Se_2 chain fragments in the parent Ph_2Se_2 crystal (YUXPIR) and co-crystal **2** (wireframe). (d) Energy framework diagram for the same 2D chain fragment of parent Ph_2Se_2 (YUXPIR). Solid blue cylinders show total energy framework (Crystal Explorer 3.1, cut off 12 kJ mol^{-1}). Black dotted lines show intermolecular contacts at the distances shorter than the respective sum of van der Waals radii.

turned out to be a "weaker link" and is substituted by I–Ph XBs (−5.9 kcal mol^{-1}) in a supramolecular reaction with DITFB, similar to **1**. This reaction can be visualized as DITFB insertion between the zig-zag chains of the parent Ph_2Se_2 energy framework (see Fig. 5).

Supramolecular insertion of *p*-DITFB stacks between the chains of Ph_2E_2 in the co-crystals **1–3** can also be presented in terms of long-range synthon Aufbau modules (LSAM[36,37]), so that columnar *p*-DITFB modules insert between the chains or columnar Ph_2E_2 modules. Both of these LSAMs can be assessed and visualized using the energy framework model of CrystalExplorer as a pair of the strongest interactions in the co-crystals **1–2** (see Tables S1–S5, ESI†). This suggests that energy frameworks can also be used for the preliminary co-crystal structure evaluation and determination of LSAMs in the crystal structures.

Co-crystallization of the Ph_2E_2 sulphur congener – diphenyl disulfide (Ph_2S_2) with *p*-DITFB, has resulted, at best, in the starting compounds. The low affinity of Ph_2S_2 for *p*-DITFB is interesting in comparison with quite the opposite trend in the supramolecular reactivity of Ph_2E_2 (E = S, Se, Te) towards the π-hole co-former, *i.e.*, the low affinity of Ph_2Te_2 and Ph_2Se_2 for octafluoronaphthalene ($C_{10}F_8$, OFNp), reported in ref. 38. It is noteworthy that only 1D chains of Ph_2S_2 in the parent crystal (which is isostructural with Ph_2Se_2) are reproduced in the co-crystal with OFNp, and in contrast to the native Ph_2Se_2/co-crystal **2** pair, the link between these 1D chains does not appear in the OFNp co-crystal (see Fig. 6).

The energy framework and LSAM approaches appear quite illustrative in this case also. The supramolecular reaction between diphenyl disulfide and octafluoronaphthalene can be

§ Total energy is a sum of intermolecular electrostatic, polarization, dispersion and exchange-repulsion energy terms.[10]

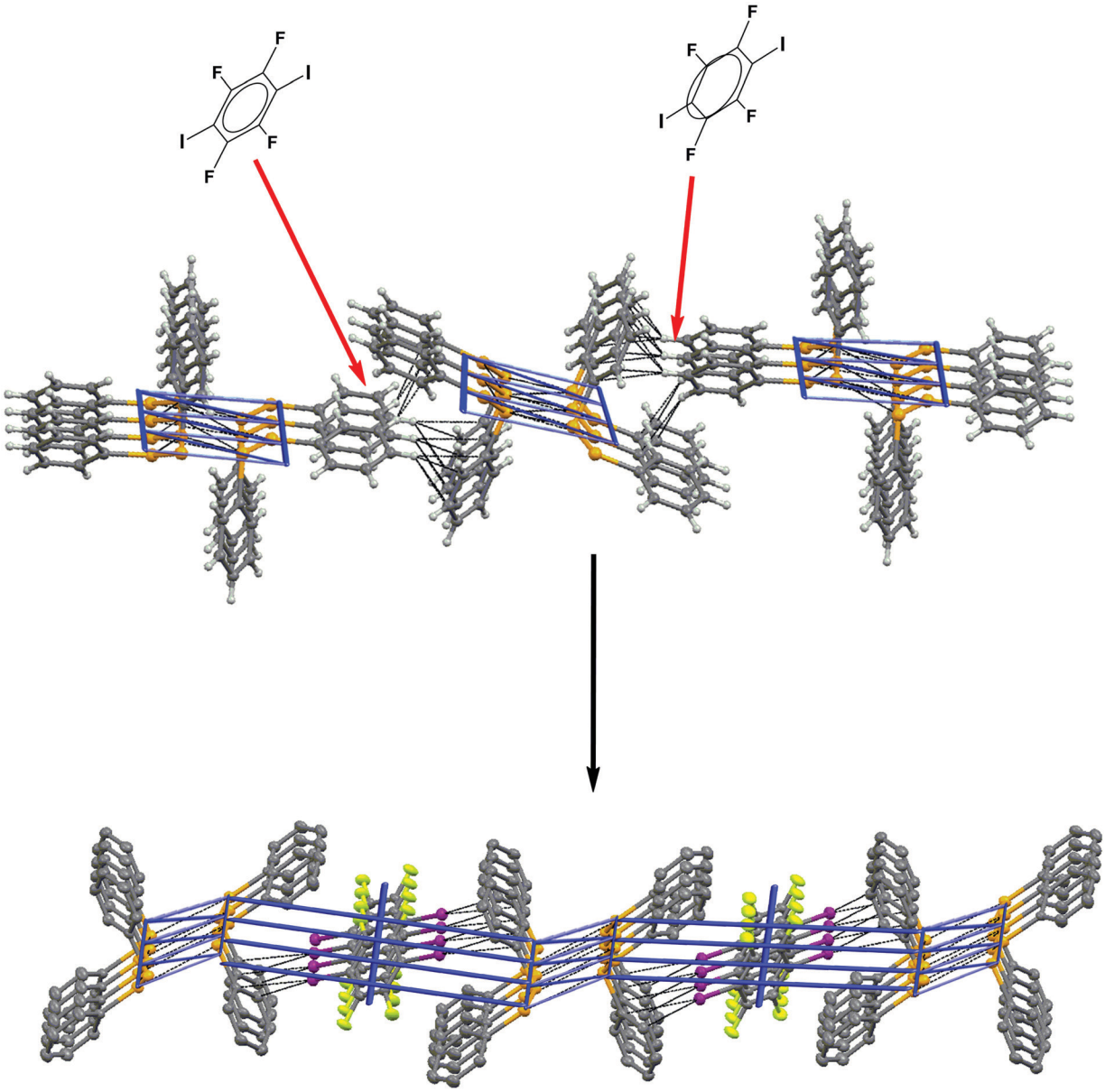

Fig. 5 Supramolecular insertion of *p*-DITFB into the voids between the 2D zig-zag chains in the energy framework (not the crystal lattice) of Ph_2Se_2 resulting in co-crystal **2**. Solid blue lines show the total energy framework (Crystal Explorer 17, cut off 12 kJ mol^{-1}). Black dotted lines show intermolecular bonding.

presented as the insertion of OFNp molecules between the 1D chain LSAMs of Ph_2S_2 (see Fig. 6 and Fig. S3, S4, ESI†). As mentioned above, the S–S interaction between these LSAMs does not re-appear in the Ph_2S_2–OFNp co-crystal, but their self-complimentary dimerization remains the same in **1**.

Some of our other "unsuccessful" co-crystallization attempts are also worth mentioning. The first to mention is the co-crystallization of Ph_2Te_2 with another efficient ditopic XB-donor conformer – diodoacetylene C_2I_2, which resulted in an oxidative addition product $PhTeI_2C{=}CTePh$[39] instead of a supramolecular assembly. The slow evaporation of Ph_2Te_2 and Ph_2Se_2 with 1,4-diodo-octafluorobutane yielded only well-formed crystals of parent Ph_2E_2. Attempted co-crystallizations of Ph_2Te_2 and Ph_2Se_2 with iodo-pentafluorobenzene, 1,2-diiodotetrafluorobenzene (*o*-DITFB) and 1,3-diiodotetrafluorobenzene (*m*-DITFB) also did not yield any crystalline material suitable for the powder or single crystal XRD analysis.

Summary

The networks of E–E and E–π (E = Se, Te) chalcogen bonds assemble Ph_2Te_2 molecules into quite stable modular 1 and 2D chain architectures, persistently reproduced in the crystals of pure Ph_2Te_2 and their co-crystals with the XB donor molecules. These relatively stable LSAM chains are associated by the weaker chalcogen and hydrogen bonds into 3D structures, which partly reproduce the longer range packing patterns of the native Ph_2E_2 crystals (see Table S6, ESI†). The latter can be

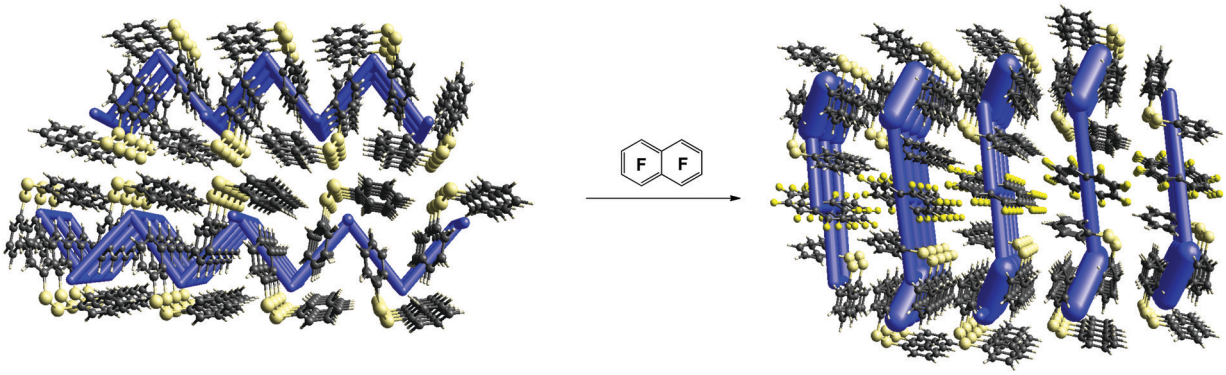

Fig. 6 Supramolecular insertion of $C_{10}F_8$ into the voids between the 2D zig-zag chains in the energy framework (not the crystal lattice) of Ph_2S_2 resulting in the Ph_2S_2–$C_{10}F_8$ co-crystal. Solid blue lines show the total energy framework (Crystal Explorer 17, cut off 15 kJ mol^{-1}).

visualized and validated using the energy framer approach of Crystal Explorer software. Accordingly, the supramolecular reaction of Ph_2E_2 with the *p*-DITFB can be presented as the insertion of the XB donor co-former columnar LSAMs between the XB-acceptors of the columnar LSAMS. This approach allows a certain degree of co-crystal structure predictability.

Presence of equally distributed M and P enantiomeric forms of Ph_2Te_2 in the Ph_2Te_2–DITFB co-crystal **1** provides an insight into the nature of conformational isomerism of diorganodichalcogens. The persistent packing pattern in both parent and binary co-crystals is another demonstration that co-crystals can be helpful in the exploration of the structural landscape of a particular compound.[40] Taking into account the reported Te–Te auto-association of organic ditelluride molecules in solution,[41] this can also give some insight into the early stages of their crystallization.

Experimental part

Solvents were purified, dried and distilled under an argon atmosphere prior to use. Commercial *p*-DITFB and Ph_2Se_2 were used without additional purification, Ph_2Te_2 (Sigma-Aldrich) was recrystallized from hexane.

Preparation of 1

41 mg (0.1 mmol) of Ph_2Te_2 and 40 mg (0.1 mmol) of *p*-DITFB were dissolved in 0.1 mL of CH_2Cl_2 in 5 mm glass tube, sealed with 2 layers of parafilm and left at room temperature in the dark. The slow diffusion of the solvent through the parafilm for 48 hours enabled in the formation of well-formed uniform orange rod-like crystals that were used for single crystal XRD analysis.

Preparation of 2

31 mg (0.1 mmol) of Ph_2Se_2 and 40 mg (0.1 mmol) of *p*-DITFB were dissolved in 0.1 mL of CH_2Cl_2 in the 5 mm glass tube placed into the 20 mm/10 mL test tube containing 2 mL of *n*-heptane in argon atmosphere, which was closed and left for 48 hours at 4 °C. Slow vapor diffusion at low temperature enabled in the formation of well-formed uniform elongated yellow prisms that were used for single crystal XRD analysis.

Computational details

Theoretical calculations were performed with the ORCA 4.01 program package,[42] using experimental crystal geometries. A non-hybrid PBE functional[43] dispersion correction with Becke–Johnson damping (D3BJ)[44] and def2-SVP basis set[45] with small-core pseudopotential for Te and I atoms[46] was used for hydrogen atom position optimization in molecular clusters cut from XRD structure. Def2/J auxiliary basis[47] was used for Coulomb fitting. Electron density calculations on resulting geometries were performed using ZORA approximation for scalar relativistic effects,[48] a hybrid functional PBE0[49] and all-electron def2-TZVP[40] basis set recontracted for ZORA. RIJCOSX approximation[50] in combination with SARC/J auxiliary basis set[42,51] was used to improve the computational speed. QTAIM analysis was performed with the AIMAll program.[52] Intermolecular interaction energies were estimated semi-qualitatively using the correlation formula $E_{int} = \approx -1/2V(r)$ between interaction energy and potential energy density at corresponding bond critical points.[53]

Energy frameworks for Ph_2Te_2 and Ph_2Se_2 were generated from the intermolecular energies calculated in CrystalExplorer 17 (TONTO, B3LYP-DGDZVP)[54] for all unique molecular pairs in the first coordination sphere of a molecule using experimental crystal geometries. For the co-crystals **1** and **2**, the above procedure has been performed twice – separately for each co-former molecule in the asymmetric unit.[55] All the electronic structure calculations for the ESP mapping of Ph_2E_2 (E = S, Se, Te) were obtained with the general gradient approximation (GGA) using the PW91[56] density functional theory (DFT) with the Zeroth Order Regular Approximation (ZORA)[57] to consider the relativistic effects implemented in the Amsterdam Density Functional (ADF) suite code.[58] In the present computation, quadruple-ζ with four polarization quality (QZ4P) quality Slater-type basis sets were used for all the atoms studied here.[59]

Crystal structure investigation of compounds 1–2

A Bruker APEX II CCD area detector diffractometer equipped with a graphite-monochromated Mo Kα radiation (0.71070 Å) was used for the cell determination and intensity data collection for compounds **1–2**. The structure was solved by direct methods

and refined by full-matrix least squares against F^2 using SHELXL-97 and Olex2 software.[60,61] Non-hydrogen atoms were refined with anisotropic thermal parameters. All hydrogen atoms were geometrically fixed and refined using a riding model. Atomic coordinates and other structural parameters of **1–2** have been deposited with the Cambridge Crystallographic Data Centre (CCDC no. 1815996 (**1**), 1815995 (**2**)).†

The powder pattern was measured on a Bruker D8 Advance Vario diffractometer at room temperature with a LynxEye detector and a Ge(111) monochromator, λ(Cu Kα1) = 1.54060 Å, $\theta/2\theta$ scan from 2° to 90°, step size 0.0104788°. The measurement was performed in the transmission mode, with the sample deposited between two Kapton films. Quantitative phase analysis was performed with the Rietveld method as implemented in Bruker TOPAS5.[62]

Conflicts of interest

There are no conflicts to declare.

Acknowledgements

The XRD experiments were performed using shared experimental facilities supported by the IGIC RAS state assignment. We acknowledge funding by the Presidium of Russian Academy of Sciences (Y. T. and I. S. – grant I.35), Department of Science and Technology, Government of India (D. K. R. – YSS/2015/000034, S. P. – Ramanujan Faculty Fellowship SB/S2/RJN-067/2017).

References

1 (*a*) H.-J. Schneider, *Angew. Chem., Int. Ed.*, 2009, **48**, 3924–3977; (*b*) G. M. Whitesides, *Angew. Chem., Int. Ed.*, 2015, **54**, 2–16.
2 S. Aitipamula, P. S. Chow and R. B. H. Tan, *CrystEngComm*, 2014, **16**, 3451.
3 G. Desiraju, *J. Am. Chem. Soc.*, 2013, **135**, 9952–9967.
4 G. Cavallo, P. Metrangolo, R. Milani, T. Pilati, A. Priimagi, G. Resnati and G. Terraneo, *Chem. Rev.*, 2016, **116**, 2478–2601.
5 W. Wang, B. Ji and Y. Zhang, *J. Phys. Chem. A*, 2009, **113**, 8132–8135.
6 S. Scheiner, *Acc. Chem. Res.*, 2013, **46**(2), 280–288.
7 C. B. Aakeroy and D. J. Salmon, *CrystEngComm*, 2005, **7**(72), 439–448.
8 C. B. Aakeroy, J. Desper, E. Elisabeth, B. Helfrich, B. Levin and J. Urbina, *Z. Kristallogr.*, 2005, **220**, 325.
9 O. V. Shishkin, V. V. Medvediev and R. I. Zubatyuk, *CrystEngComm*, 2013, **15**, 160–167.
10 M. J. Turner, S. P. Thomas, M. W. Shi, D. Jayatilaka and M. A. Spackman, *Chem. Commun.*, 2015, **51**, 3691–3928.
11 M. J. Turner, J. J. McKinnon, S. K. Wolff, D. J. Grimwood, P. R. Spackman, D. Jayatilaka and M. A. Spackman, *CrystalExplorer17*, University of Western Australia, 2017.
12 S. Bhandary, A. Sirohiwal, R. Kadu, S. Kumar and D. Chopra, *Cryst. Growth Des.*, 2018, **18**, 3734–3739.
13 M. I. Bruce, N. J. Head, B. W. Skelton, M. A. Spackman and A. H. White, *Aust. J. Chem.*, 2018, **71**, 70–73.
14 M. W. Shi, S. P. Thomas, G. A. Koutsantonis and M. A. Spackman, *Cryst. Growth Des.*, 2015, **15**(12), 5892–5900.
15 D. Dey, S. Bhandary, S. P. Thomas, M. A. Spackman and D. Chopra, *Phys. Chem. Chem. Phys.*, 2016, **18**, 31811–31820.
16 S. P. Thomas, M. W. Shi, G. A. Koutsantonis, D. Jayatilaka, A. J. Edwards and M. A. Spackman, *Angew. Chem.*, 2017, **129**, 1–6.
17 S. P. Thomas, M. W. Shi, D. Jayatilaka and M. A. Spackman, *Acta Crystallogr., Sect. A: Found. Adv.*, 2017, **73**, C849.
18 K. K. Jha, S. Dutta, V. Kumarb and P. Munshi, *CrystEngComm*, 2016, **18**, 8497–8505.
19 C. Wang, S. Paul, K. Wang, S. Hu and C. C. Sun, *Cryst. Growth Des.*, 2017, **17**(11), 6030–6040.
20 C. Wang and C. C. Sun, *Cryst. Growth Des.*, 2018, **18**(3), 1909–1916.
21 B. Raju, S. Ranjan, V. S. Vishnu, M. Bhattacharya, B. Bhattacharya, A. K. Mukhopadhyay and C. M. Reddy, *Cryst. Growth Des.*, 2018, **7**, 3927–3937.
22 C. F. Macrae, P. R. Edgington, P. McCabe, E. Pidcock, G. P. Shields, R. Taylor, M. Towler and J. van de Streek, *J. Appl. Cryst.*, 2006, **39**, 453–457, DOI: 10.1107/S002188980600731X.
23 P. Politzer, J. S. Murray and M. C. Concha, *J. Mol. Model.*, 2008, **14**, 659–665.
24 A. Bauzá, I. Alkorta, A. Frontera and J. Elguero, *J. Chem. Theory Comput.*, 2013, **9**(11), 5201–5210.
25 A. Bauzá, D. Quiñonero, P. M. Deyà and A. Frontera, *CrystEngComm*, 2013, **15**, 3137–3144.
26 L. Vogel, P. Wonner and S. M. Huber, *Angew. Chem., Int. Ed.*, 2018, **58**, 1880–1891.
27 C. B. Aakeröy, T. K. Wijethunga, J. Desper and M. Đaković, *Cryst. Growth Des.*, 2016, **16**(5), 2662–2670.
28 E. Espinosa, E. Molins and C. Lecomte, *Chem. Phys. Lett.*, 1998, **285**, 170–173.
29 I. V. Ananyev, V. A. Karnoukhova, A. O. Dmitrienko and K. A. Lyssenko, *J. Phys. Chem.*, 2017, **121**, 4517–4522.
30 L. N. Puntus, K. A. Lyssenko, M. Y. Antipin and J.-C. G. Buenzli, *Inorg. Chem.*, 2008, **47**, 11095–11107.
31 A. O. Borissova, A. A. Korlyukov, M. Y. Antipin and K. A. Lyssenko, *J. Phys. Chem.*, 2008, **112**, 11519–11522.
32 S. Z. Vatsadze, A. V. Medved'ko, N. V. Zyk, A. L. Maximov, S. A. Kurzeev, G. M. Kazankov and K. A. Lyssenko, *Organometallics*, 2009, **28**, 1027–1031.
33 A. O. Borissova, M. Y. Antipin, D. S. Perekalin and K. A. Lyssenko, *CrystEngComm*, 2008, **10**, 827–832.
34 C. F. Mackenzie, P. R. Spackman, D. Jayatilaka and M. A. Spackman, *IUCrJ*, 2017, **4**, 575–587.
35 A. L. Fuller, L. A. S. Scott-Hayward, Y. Li, M. Buhl, A. M. Z. Slawin and J. D. Woollins, *J. Am. Chem. Soc.*, 2010, **132**, 5799.
36 P. Ganguly and G. R. Desiraju, *CrystEngComm*, 2010, **12**, 817–833.
37 A. Mukherjee, *Cryst. Growth Des.*, 2015, **15**, 3076–3085, DOI: 10.1021/acs.cgd.5b00242.
38 I. Y. Bagryanskaya, Y. V. Gatilov, E. Lork, R. Mews and A. V. Zibarev, *J. Fluorine Chem.*, 2006, **127**, 746–754.

39 Y. V. Torubaev, A. A. Pasynskii, A. V. Pavlova and M. M. Shaikh, *Mendeleev Commun.*, 2017, **27**(2), 141–143.
40 A. Mukherjee, *Cryst. Growth Des.*, 2015, **15**, 3076–3085, DOI: 10.1021/acs.cgd.5b00242.
41 P. J. W. Elder and I. Vargas-Baca, *Phys. Chem. Chem. Phys.*, 2016, **18**, 30740–30747.
42 F. Neese, *Software update: the ORCA program system, version 4.0*, Wiley Interdisciplinary Reviews: Computational Molecular Science, 2017, p. e1327, DOI: 10.1002/wcms.1327.
43 (*a*) J. P. Perdew, K. Burke and M. Ernzerhof, *Phys. Rev. Lett.*, 1996, **77**, 3865; (*b*) J. P. Perdew, K. Burke and M. Ernzerhof, *Phys. Rev. Lett.*, 1997, **78**, 1396.
44 (*a*) S. Grimme, S. Ehrlich and L. Goerigk, *J. Comput. Chem.*, 2011, **32**, 1456; (*b*) S. Grimme, J. Antony, S. Ehrlich and H. Krieg, *J. Chem. Phys.*, 2010, **132**, 154104.
45 F. Weigend and R. Ahlrichs, *Phys. Chem. Chem. Phys.*, 2005, **7**, 3297.
46 K. A. Peterson, D. Figgen, E. Goll, H. Stoll and M. Dolg, *J. Chem. Phys.*, 2003, **119**, 11113–11123.
47 F. Weigend, *Phys. Chem. Chem. Phys.*, 2006, **8**, 1057.
48 (*a*) E. van Lenthe, E. J. Baerends and J. B. Snijders, *J. Chem. Phys.*, 1993, **99**, 4597; (*b*) C. van Wüllen, *J. Chem. Phys.*, 1998, **109**, 392.
49 C. Adamo and V. Barone, *J. Chem. Phys.*, 1999, **110**, 6158–6170.
50 (*a*) S. Phan, E. Kierlik and M. L. Rosinberg, *J. Chem. Phys.*, 1993, **99**, 4597; (*b*) C. van Wüllen, *J. Chem. Phys.*, 1998, **109**, 392.
51 D. A. Pantazis and F. Neese, *Theor. Chem. Acc.*, 2012, **131**, 1292.
52 T. A. Keith, *AIMALL, version 16.01.09*, http://aim.tkgristmill.com/.
53 E. Espinosa, E. Molins and C. Lecomte, *Chem. Phys. Lett.*, 1998, **285**, 170.
54 M. J. Turner, S. P. Thomas, M. W. Shi, D. Jayatilaka and M. A. Spackman, *Chem. Commun.*, 2015, **51**, 3691–3928.
55 http://130.95.176.70/wiki/index.php?titl=Intermolecular_Interaction_Energies.
56 J. P. Perdew, J. A. Chevary, S. H. Vosko, K. A. Jackson, M. R. Pederson, D. J. Singh and C. Fiolhais, *Phys. Rev. B: Condens. Matter Mater. Phys.*, 1992, **b**, 6671–6687.
57 (*a*) E. van Lenthe, A. Ehlers and E. J. Baerends, *J. Chem. Phys.*, 1999, **110**, 8943–8953; (*b*) E. Van Lenthe, J. G. Snijders and E. J. Baerends, *J. Chem. Phys.*, 1996, **105**, 6505–6516.
58 G. te Velde, F. M. Bickelhaupt, E. J. Baerends, C. Fonseca Guerra, S. J. A. van Gisbergen, J. G. Snijders and T. Ziegler, *J. Comput. Chem.*, 2001, **22**, 931–967.
59 E. van Lenthe and E. J. Baerends, *J. Comput. Chem.*, 2003, **24**, 1142.
60 G. M. Sheldrick, *Acta Crystallogr., Sect. A: Found. Crystallogr.*, 2008, **64**, 112.
61 O. V. Dolomanov, L. J. Bourhis, R. J. Gildea, J. A. K. Howard and H. Puschmann, *J. Appl. Crystallogr.*, 2009, **42**, 339–341.
62 *TOPAS 5 User Manual*, BrukerAXS GmbH, Karlsruhe, Germany, 2015.